JTTEE5 19:975–989
DOI: 10.1007/s11666-010-9481-4
1059-9630/$19.00 © ASM International

Structural Analysis of Cold-Sprayed Nickel-Based Metallic and Metallic-Ceramic Coatings

Heli Koivuluoto and Petri Vuoristo

(Submitted October 31, 2009; in revised form December 29, 2009)

In cold spraying, many factors, e.g., powder characteristics and compositions, spraying parameters, and post-treatments affect coating formation. Cold spraying is the optimal technique to produce highly dense coatings. Furthermore, denseness and impermeability are the criterions for the corrosion resistance of anodically protective coatings. Therefore, this study focuses on denseness improvement of cold-sprayed (CS) metallic coatings. The aim of this study was to characterize structural details of CS Ni, Ni-20Cu, Ni-20Cr, Ni-20Cr + Al_2O_3, and Ni-20Cr + WC-10Co-4Cr coatings in order to produce dense coatings by optimizing the affecting factors. Denseness of Ni coating was improved with optimized spraying parameters whereas denseness of Ni-20Cr coatings was increased with added hard particles in the powder mixture. In addition, denseness of Ni-20Cu coatings was improved by heat treatments. Denseness of the coatings is evaluated by corrosion tests. In addition, fracture behavior, microstructures, and hardness studies of the coatings are performed.

Keywords coating structure, cold spraying, denseness, heat treatment of coatings, Ni alloy coatings

1. Introduction

Cold spraying is a solid-state process wherein the coating is formed by powder particle impacts with a high kinetic energy and thus, with a high particle velocity (Ref 1, 2). In addition, ceramic particles with a metallic matrix can be sprayed using the cold spray system. At least one component of the sprayed powder needs to be ductile (Ref 3). During impacts, powder particles deform plastically and adhere to the substrate surface or to other particles and form the coating (Ref 4, 5). Formation of bonds between particles requires critical impact velocities of particles in order to obtain adequate bonding and adhesion (Ref 1). Furthermore, successful particle-substrate and particle-particle bonding requires a high level of plastic deformation and adiabatic shear instability. In addition, strong adhesion between particles requires the formation of material jets due to the thermal softening. Higher particle velocity leads stronger bonding and thus, affects the denseness of coatings (Ref 2). Cold spraying is a potential method of spraying dense (very low porosity) coatings for applications where corrosion protection is needed. Denseness and impermeability depend strongly on spraying process conditions, powder characteristics, and coating material, and moreover, the combination of these affecting factors (Ref 6). Additionally, coating quality relies on spraying conditions, higher velocity leads to stronger plastic deformation and furthermore, coating structure become denser and mechanical properties are improved (Ref 7, 8). The preheating temperature of process gas reportedly has influence on the coating quality. Higher temperature together with higher pressure leads to denser coating structure due to the thermal softening and local shear instability (Ref 1, 2).

Metal-ceramic composite coatings are reportedly produced by using cold spray processes (Ref 9-11). Furthermore, hardmetal coatings, e.g., WC-Co coatings have been prepared with the cold spraying (Ref 12, 13). Adhesion of metallic particles depends on particle velocity and temperature on impact. These parameters affect also the behavior of hard particles (e.g., erosion, activation, and sticking) (Ref 9). Ceramic particles activate the sprayed surface by removal of oxide layers of metallic particles. This improves the deposition efficiency. On the other hand, hard particles hammer the sprayed particles, providing a denser coating structure (Ref 14). However, the amount of ceramic particles in the sprayed coating is low compared to the initial powder composition. Usually, coatings contain ceramic particles below 5% from total amount of ceramic powder (Ref 11, 15). Hard particles can have higher or lower velocity than the metallic particles in the powder mixture. Velocity depends on powder characteristics (e.g., particle size) of the hard particles (Ref 9). Klinkov et al. (Ref 9) have shown that fine SiC particles (5 and 15 μm) have higher velocity than Al or Cu particles. However, a shock layer near to the surface decreases the velocity of 5 μm particles and thus, less

Heli Koivuluoto and **Petri Vuoristo**, Department of Materials Science, Tampere University of Technology, Tampere, Finland. Contact e-mail: heli.koivuluoto@tut.fi.

activation occurs with these particles in comparison with 15 μm particles (Ref 9). For a dense coating and tight bonds between particles, metal-metal bonding and material jet formation are required. This needs clean contact surfaces under high pressure conditions (Ref 3, 16, 17). For that, oxide layers of powder particles should be destroyed and removed from the metal surface on the impacts (Ref 18). This occurs with high plastic deformation and materials jets (Ref 3, 16-18). Removal of oxide layer can be illustrated with an egg-cell-model (during impact, particles behave similar like egg, hard cell (oxide) breaks down and soft inside (metal) deforms). After the oxide layer is broken down, a gas flow removes the oxides away (Ref 18).

Typically, the level of plastic deformation is detected from an etched microstructure of cold-sprayed (CS) coatings by the flattening degree of the particles. On the other hand, generally, material properties depend on their microstructure which in turns depends on grain structure and treatments. Therefore, plastic deformation is due to dislocation movements caused by critical shear stress. In principle, plastic deformation occurs in each grain in the individual powder particle which means that particle boundaries can restrict the deformation of some grains. This indicates different levels of plastic deformation in the particle and hence, through the coating structure (Ref 19).

The aim of this study was to investigate the structural properties of nickel-based metallic and metallic-ceramic coatings in order to improve the denseness and impermeability of these coatings. Ni, Ni-20Cu (NiCu), and Ni-20Cr (NiCr) were chosen because of their possibility to act as corrosion barrier coatings. In addition, hard Al_2O_3 and WC-10Co-4Cr (WC-Co-Cr) particles were mixed with the NiCr powder in order to decrease porosity and increase denseness of the coatings. The corrosion resistance of these coatings depends on denseness (existing through-porosity, impermeability) and chemical homogeneity. It can be said that microstructure of these coatings defines their corrosion protection capability. This study sought structural properties such as microstructures, fracture surfaces, corrosion properties, and mechanical properties of the CS Ni, NiCu, NiCr, NiCr + 50(vol.%)Al_2O_3, and NiCr + 30(vol.%)WC-Co-Cr coatings. In addition, the effects of spraying parameters and heat treatment as a post-treatment were studied.

2. Experimental Techniques

Ni, Ni20Cu, Ni20Cr, Ni20Cr + 50Al_2O_3, and Ni20Cr + 30WC-Co-Cr powders were CS with different spraying parameters. Metallic powders were gas-atomized having a spherical shape whereas added hard particles (Al_2O_3 and WC-Co-Cr) had an irregular blocky shape. Al_2O_3 powder was fused and crushed and WC-Co-Cr powder sintered and crushed. Table 1 shows powder characteristics and Fig. 1 morphologies of the powders used. Particle sizes are nominal given by supplier. Metallic-ceramic powder mixtures were manually mixed by hand.

Coatings were prepared at Linde AG Linde Gas Division (Unterschleissheim, Germany) with a CGT Kinetiks 4000 high-pressure cold spray system. Table 2 summarizes the spraying parameters used in this study. Two different beam distance-traverse speed combinations were tested with each powder (except NiCr). In addition to these, three different preheating temperatures of gas (500, 600, and 700 °C) were tested with the NiCr + 30WC-Co-Cr powder. In all experiments, nitrogen was used as a process gas. Substrates, carbon steel sheets (50 × 100 × 1.5 mm^3), were grit-blasted (1 mm Al_2O_3 grits) prior to spraying.

Cold-sprayed coatings were characterized both in the as-sprayed and heat-treated state. Heat treatments were done using a furnace in a protective (Ar-3%H_2) atmosphere. Figure 2 shows the heat treatment procedure with three different regions. The region I is the temperature rising up to the temperature of 600 °C, II the temperature holding with the holding time of 2 h at 600 °C, and III the temperature cooling. Samples were in the protective atmosphere during total heat treatment cycle. Heat treatment temperature of 600 °C was chosen according to our previous studies of CS Ni coatings (Ref 20) and Ni20Cr coatings (Ref 21).

Powder morphologies were characterized using a Philips XL30 scanning electron microscope (SEM). Coating structures and fracture surfaces were analyzed with a Zeiss ULTRAplus field-emission scanning electron microscope (FESEM). Microstructures were studied from unetched metallographic cross-sectional samples. Coating samples were bent for fracture surface analysis. Hard particle fractions were calculated from the coating cross sections using image analysis (ImageJ). Coating denseness and especially existing through-porosity were studied using open-cell electrochemical potential measurements and salt spray tests. The electrochemical cell used in the open-cell potential measurements consisted of a plastic tube, of diameter 20 mm and volume 12 mL, glued on the surface of the coating specimen. A 3.5 wt.% NaCl solution was placed in the tube for 9-day measurements. Open-cell potential measurements were taken with a Fluke 79 III true RMS multimeter. A silver/silver chloride (Ag/AgCl) electrode was used as a reference electrode. The salt spray test was done according to the ASTM B117 standard. Substrates were masked with epoxy paint before testing in order to allow the coating surfaces to be in contact only with the corroding salt spray. A 5 wt.% NaCl solution was used with an exposure time of 96 h, a temperature of 35-40 °C, a solution

Table 1 Powder characteristics

Powder	Particle size, μm	Production method	Supplier
Ni	−30 + 10	Gas-atomized	H.C. Starck
Ni-20Cu	−30 + 10	Gas-atomized	Sandvik Osprey
Ni-20Cr	−30 + 10	Gas-atomized	Sandvik Osprey
Al_2O_3	−90 + 45	Fused and crushed	H.C. Starck
WC-10Co-4Cr	−45 + 11	Sintered and crushed	Sulzer Metco

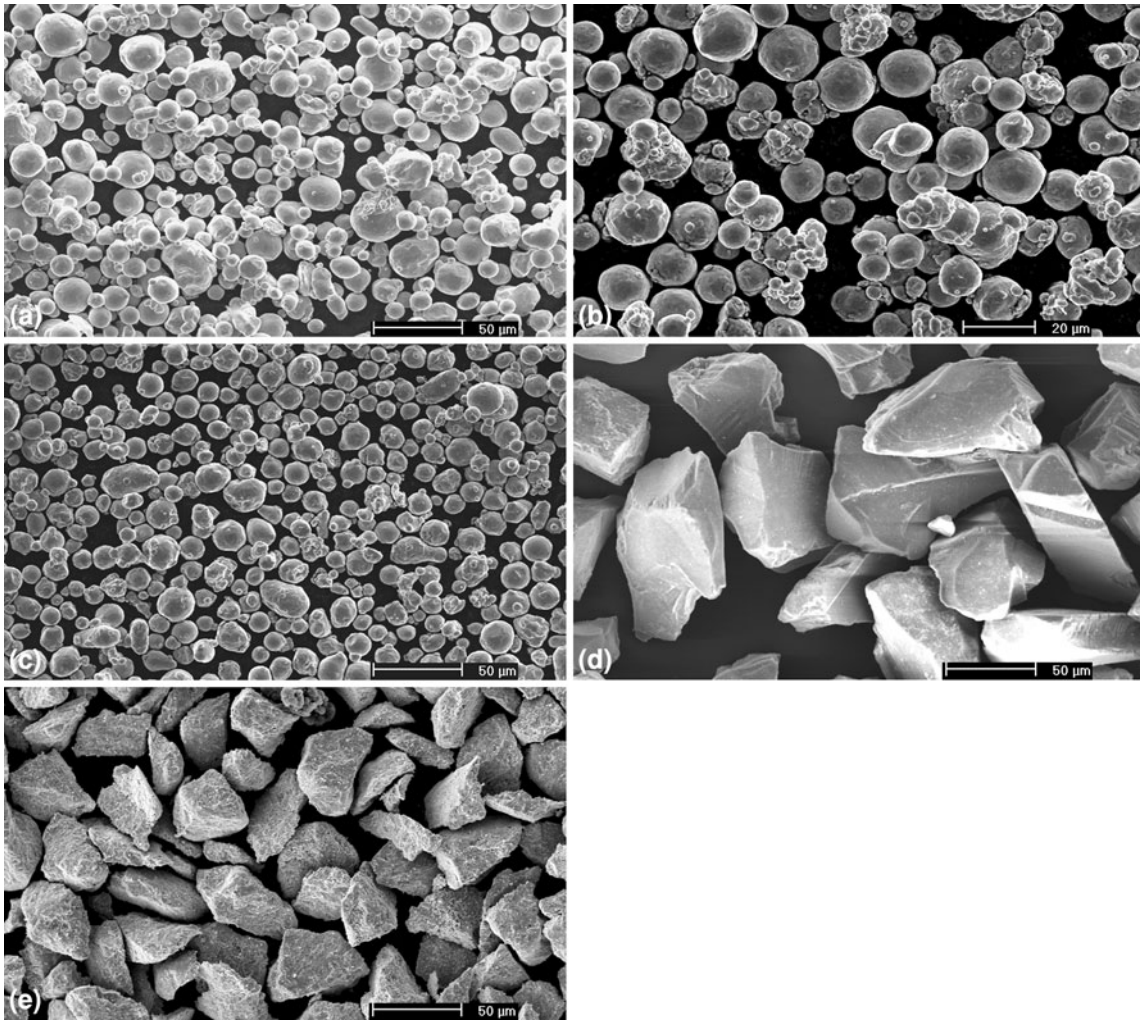

Fig. 1 Morphologies of (a) Ni (−30 + 10 μm), (b) Ni20Cu (−30 + 10 μm), (c) Ni20Cr (−30 + 10 μm) metallic powders and added hard particles, (d) Al_2O_3 (−90 + 45 μm), and (e) WC-10Co-4Cr (−45 + 11 μm). SEM images

Table 2 Spraying parameters

Coating	Gas pressure, bar	Gas temperature, °C	Gas flow, m^3/h	Beam distance, mm	Traverse speed, m/min
Ni-1	36	700	82	0.75	40
Ni-2	36	700	82	1.5	20
NiCu-1	39	650	89	0.75	40
NiCu-2	39	650	89	1.5	20
NiCr-1	38	600	89	0.75	40
NiCr + 50Al_2O_3-1	39	700	88	0.75	40
NiCr + 50Al_2O_3-2	39	700	88	1.5	20
NiCr + 30WC-Co-Cr-1	37	700	80	0.75	40
NiCr + 30WC-Co-Cr-2	37	700	80	1.5	20
NiCr + 30WC-Co-Cr-3	37	500	88	0.75	40
NiCr + 30WC-Co-Cr-4	37	600	84	0.75	40

Beam distance means distance between two adjacent spray beads

pH of 6.3, and a solution accumulation of 0.04 mL/cm^2 h. Surfaces of the coatings were analyzed visually and amounts (%) of corrosion spots were characterized using image analysis (ImageJ). Vickers hardness ($HV_{0.3}$) was measured as an average of ten measurements with a Matsuzawa hardness tester.

3. Results

The corrosion tests show clearly denseness and impermeability or existing through-porosity and therefore, weak bonding or structural defects in the coating structures (Ref 22). The densification effect of added hard Al_2O_3 particles on the denseness of the $NiCr + Al_2O_3$ coatings was clearly showed in the previous study (Ref 14). Denseness improvement was noticeable due to the hammering effect of hard particles together with possibility to use higher process temperature without clogging the nozzle (Ref 14). The main focus point of this study was to improve denseness in order to decrease through-porosity (open-porosity or interconnected porosity). Denseness, fracture behavior, microstructure, and hardness of these CS Ni, NiCu, NiCr, $NiCr + Al_2O_3$, and NiCr + WC-Co-Cr coatings were characterized.

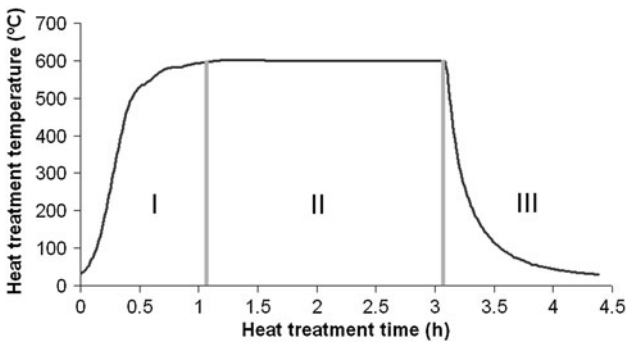

Fig. 2 Heat treatment procedure: (I) temperature rising, (II) temperature holding, and (III) temperature cooling

3.1 Denseness

Open-cell potential measurements and salt spray tests were done in order to investigate the impermeability of the coatings, i.e., is the coating impermeable or is there existing through-porosity (in the other words open-porosity or interconnected porosity) in the coating structures. The corrosion resistance of these coatings is based on anodic protection and hence, fully dense coating structure is the requirement. The results of the open-cell potential measurements are shown in Fig. 3 to 6. If the open-cell potential of the coating is close to the bulk material, it reflects the dense structure of the coating and hence, similar protection with bulk material. On the other hand, if the open-cell potential of the coating approaches the value of the substrate material, it reflects existing through-porosity in the coating structure, indicating open way for the salt solution to penetrate from coating surface to the interface between coating and substrate. The open-cell potential of as-sprayed and heat-treated Ni-1 and Ni-2 coatings, Ni bulk, and Fe52 substrate material are presented in Fig. 3.

Figure 4 shows the open-cell potential values of as-sprayed and heat-treated NiCu-1 and NiCu-2 coatings, Ni-30Cu bulk material, and Fe52 substrate material. Heat treatment improved the denseness of these coatings. The open-cell potential behavior of heat-treated coatings was closer to the bulk material compared with the substrate material, indicating denser coating structure. In addition, it should be noticed that spraying parameters had not as strong effect on the open-cell potential behavior of NiCu as with Ni coatings, reflecting that spraying parameters together with powder characteristics are strongly material-dependent in the cold spraying (Ref 6).

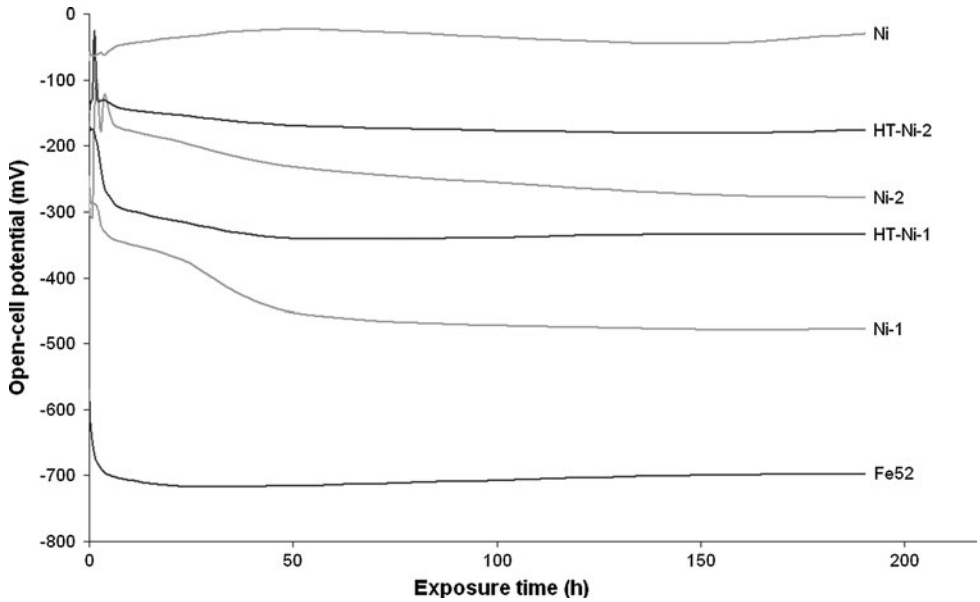

Fig. 3 Open-cell potentials of as-sprayed Ni-1 and Ni-2 coatings, heat-treated HT-Ni-1 and HT-Ni-2 coatings, Ni bulk material, and Fe52 substrate material as a function of exposure time in 3.5% NaCl solution. Ag/AgCl reference electrode

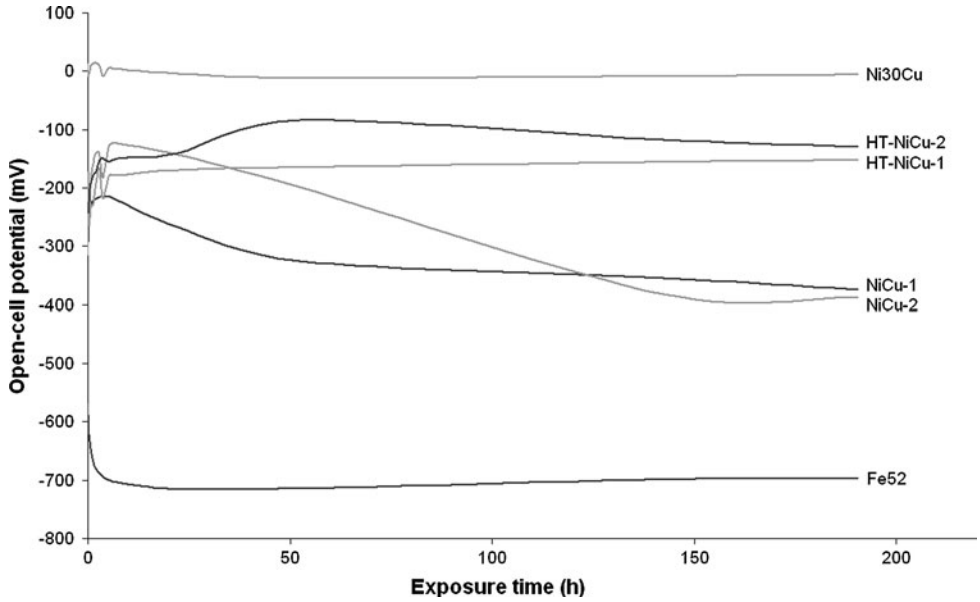

Fig. 4 Open-cell potentials of as-sprayed NiCu-1 and NiCu-2 coatings, heat-treated HT-NiCu-1 and HT-NiCu-2 coatings, Ni-30Cu bulk material and Fe52 substrate material as a function of exposure time in 3.5% NaCl solution. Ag/AgCl reference electrode

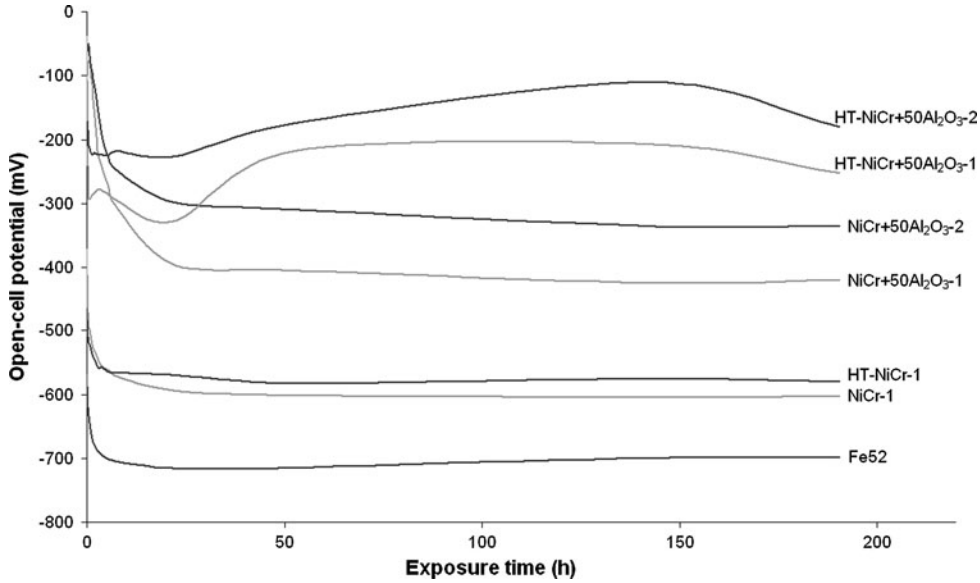

Fig. 5 Open-cell potentials of as-sprayed NiCr-1, $NiCr + 50Al_2O_3$-1 and $NiCr + 50Al_2O_3$-2 coatings, heat-treated HT-NiCr-1, HT-$NiCr + 50Al_2O_3$-1 and HT-$NiCr + 50Al_2O_3$-2 coatings and Fe52 substrate material as a function of exposure time in 3.5% NaCl solution. Ag/AgCl reference electrode

An addition of Al_2O_3 particles into the NiCr powder improved the denseness of the coating. The open-cell potential values of as-sprayed and heat-treated $NiCr + Al_2O_3$ and NiCr coatings and Fe52 substrate material are presented in Fig. 5. Pure NiCr coating contained through-porosity, and the denseness was increased with the ceramic particle addition. In addition, the improving effect of the heat treatments on denseness was noticeable also with $NiCr + 50Al_2O_3$ coatings. Our previous study (Ref 14) showed similar results of influence of the hard particle addition on coating structure. However, it should be notice that in this present study different NiCr powder was used, $-30 + 10$ μm instead of $-22.5 + 10$ μm. This provides crucial effect of powder-type together with spraying parameters (and optimal combinations of these factors) on the production of dense coatings.

Figure 6 presents the open-cell potential values of $NiCr + 30$WC-Co-Cr coatings in the as-sprayed and heat-treated state. The same effect of the hardmetal particles as the Al_2O_3 particles on the denseness improvement was

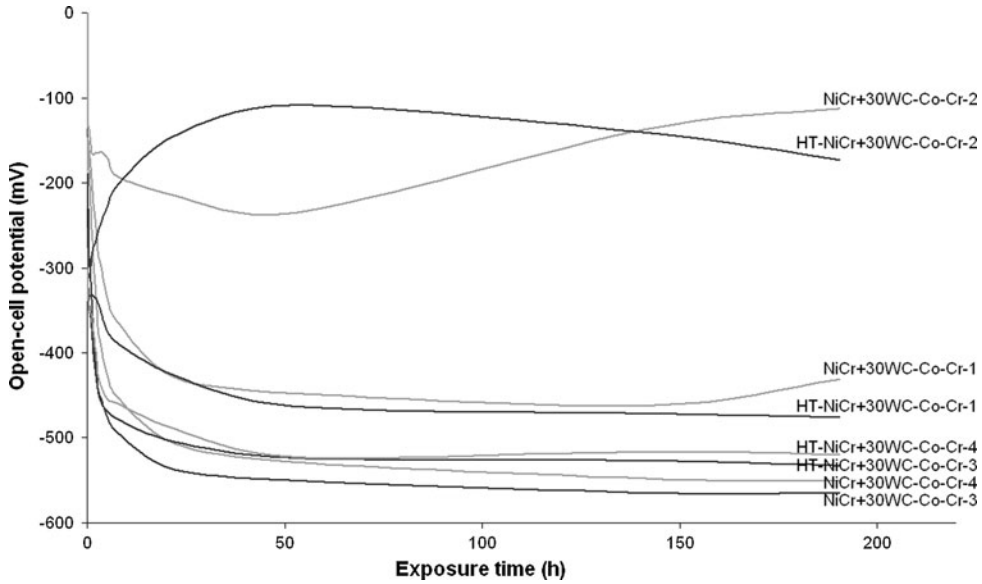

Fig. 6 Open-cell potentials of as-sprayed NiCr + 30WC-Co-Cr-1, NiCr + 30WC-Co-Cr-2, NiCr + 30WC-Co-Cr-3 and NiCr + 30WC-Co-Cr-4 coatings and heat-treated HT-NiCr + 30WC-Co-Cr-1, HT-NiCr + 30WC-Co-Cr-2, HT-NiCr + 30WC-Co-Cr-3, and HT-NiCr + 30WC-Co-Cr-4 coatings as a function of exposure time in 3.5% NaCl solution. Ag/AgCl reference electrode

Table 3 Amount of corrosion spots on the coating surface after salt spray test

	Amount of corrosion spots, %	
Coating	**As-sprayed**	**Heat-treated**
Ni-1	67.9	23.8
Ni-2	0.8	0.1
NiCu-1	54.2	11.9
NiCu-2	34.7	11.3
NiCr-1	98.5	98.9
NiCr + 50Al_2O_3-1	14.1	7.5
NiCr + 50Al_2O_3-2	12.7	8.5
NiCr + 30WC-Co-Cr-1	30.7	49.2
NiCr + 30WC-Co-Cr-2	24.7	30.0
NiCr + 30WC-Co-Cr-3	93.9	91.3
NiCr + 30WC-Co-Cr-4	67.1	97.7

observed. However, the influence of spraying parameters came clearly up with these NiCr + 30WC-Co-Cr coatings. Coatings sprayed with lower preheating temperatures (500 and 600 °C) and higher traverse speed (40 m/min versus 20 m/min) together with lower beam distance (0.75 mm versus 1.5 mm) contained more through-porosity inside the structure.

Salt spray tests showed corresponding results with the open-cell potential measurements. Table 3 shows the amount of corrosion spots analyzed by image analysis from the coating surfaces after the salt spray test. Two trends were seen in the results; (1) the heat treatment decreased the amount of corrosion spots with all coatings except NiCr + 30WC-Co-Cr coatings, and (2) the amount

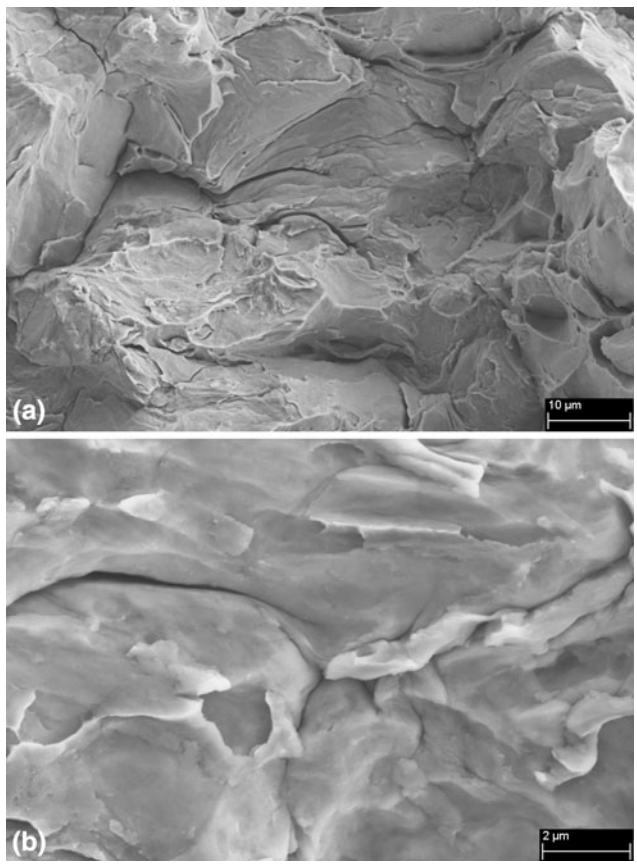

Fig. 7 Fracture surfaces of as-sprayed Ni-2 coating (a) general view and (b) crossing point of three Ni particles. FESEM images

of corrosion spots decreased with lower traverse speed and higher beam distance.

3.2 Fracture Surfaces

Fracture surface analysis was found to be a relevant method of evaluating microstructural details of the coatings. First, fracture surfaces were showed brittle and ductile fracturing behavior. Second, microscopic features, e.g., particle deformation, voids in the structure, material jets, particle bonds, and even interparticle structures were observed. As is shown in our previous studies (Ref 14, 22), existing through-porosity in the CS coatings is caused by the weak bonds between particles due to the undeformed or less deformed particles. This was seen also with the fracture surface of Ni-1 coating from which less deformed particles (spherical particles) were observed. The denseness of the CS Ni coating was improved by changing spraying parameters. With lower traverse speed and higher beam distance, coating structure became denser; see Ni-2 coating (Fig. 3 and Table 3). In addition, the higher level of plastic deformation was observed in the fracture surface (Fig. 7). Furthermore, Fig. 7(b) shows tight bonding between three Ni particles.

The fracture surface of heat-treated Ni-2 coating is presented in Fig. 8. The coating became stiffer after the heat treatment, indicating recrystallization occurred during annealing. The fracture surface of heat-treated coating was mostly ductile type whereas as-sprayed coating was partly brittle and partly ductile ruptured. The grain structure is perceived from Fig. 8(b). Figure 9 shows the fracture surfaces of NiCu-2 coatings both in the as-sprayed and heat-treated state. The strong deformation is observed in the NiCu-2 coating in Fig. 9(a). Additionally, more ductile fracture behavior (due to recrystallization) in the heat-treated state is seen in both NiCu coatings (NiCu-2 in Fig. 9b).

NiCr coatings contained porosity in their structure according to the corrosion tests. In addition to these, the fracture surfaces (Fig. 10) revealed that the deformation level was not as high as it should be (particles were not flattened enough), indicating weak bonds between particles and even pores in the particle boundaries. Heat-treated NiCr coating had similar fracture behavior with as-sprayed coating. Therefore, it can be said that heat treatment did not densify the structure due to the high amount of porosity in the boundaries. Heat-treated structure was slightly ductile, however, not as much as other coatings in this study.

The fracture surfaces of $NiCr + 50Al_2O_3$-2 coating in the as-sprayed state are presented in Fig. 11. Bonding between metallic and ceramic particles is received from

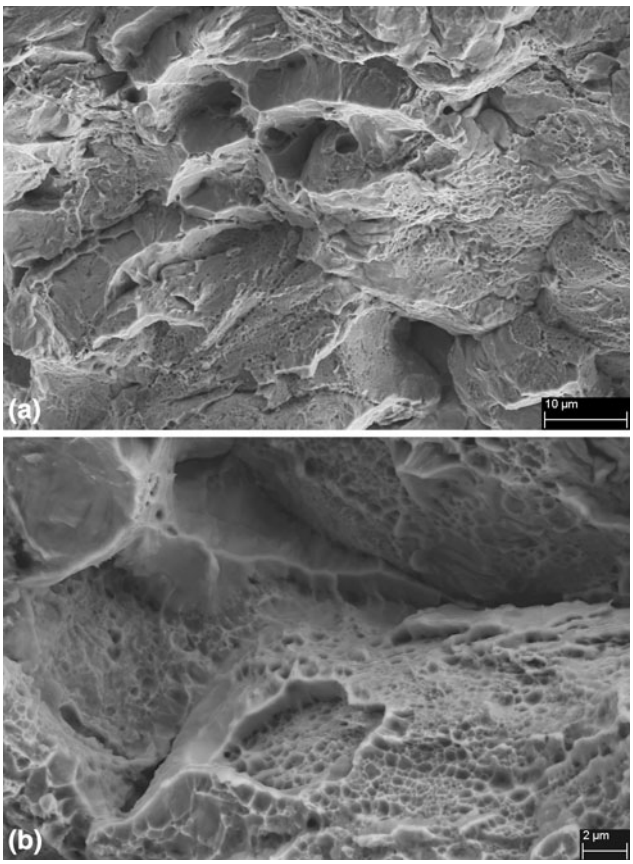

Fig. 8 Fracture surfaces of heat-treated Ni-2 coating (a) general view and (b) ductile fracture. FESEM images

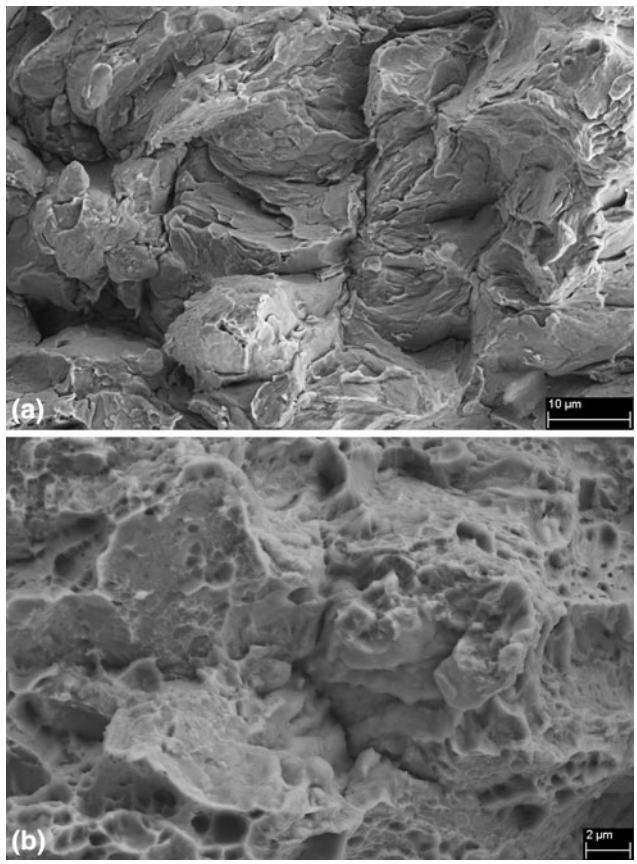

Fig. 9 Fracture surfaces of (a) as-sprayed NiCu-2 and (b) heat-treated NiCu-2 coatings. FESEM images

fracture surfaces and seemed to be tight. Arrows shows the interfaces between NiCr and Al_2O_3 particles. In addition, from Fig. 11(b), the hammering effect of the hard particles can be seen by the high level of deformation and the material jets formation of NiCr particle (NiCr particle below Al_2O_3 particle). Hard particles hammer or tamp the previous particles, densifying the entire coating structure.

Another solution to improve the denseness of NiCr coatings was to add hardmetal, WC-Co-Cr, particles into the NiCr powder. The fracture surfaces showed that the hardmetal particles broke down on the impacts. Therefore, WC-Co-Cr particles were scattered inside the structure. Figure 12 shows the fracture surfaces of NiCr + 30WC-Co-Cr-2 coatings (as-sprayed). Also here, the hammering (tamping) effect of hard particles can be seen in the closed view (Fig. 12b). After heat treatment, the fracture plane became more ductile also in this case.

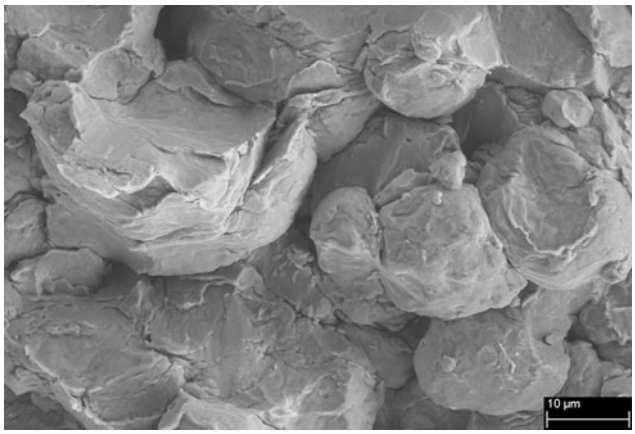

Fig. 10 Fracture surfaces of as-sprayed NiCr-1 coating. FESEM image

3.3 Microstructures

Cold-sprayed coatings are typically dense and porosity-free according to the microscopic observations. However, the corrosion tests appeared existing through-porosity in the CS Ni and Ni-30Cu coatings (Ref 22). In this study, the denseness improvement was done by optimizing powders and spraying parameters and in addition to these, with the heat treatments. The as-sprayed microstructure of Ni-2

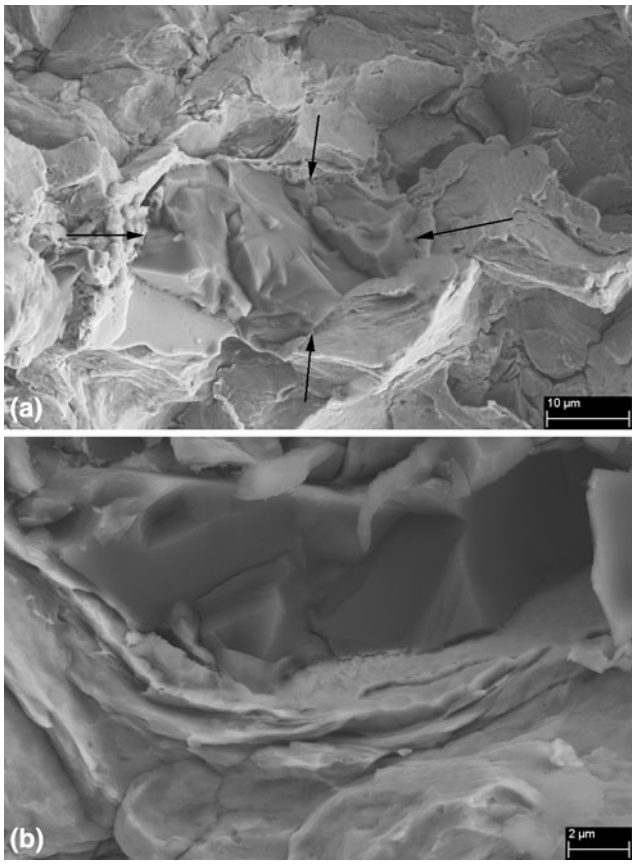

Fig. 11 Fracture surfaces of as-sprayed NiCr + 50Al_2O_3-2 coatings (a) general view; arrows indicate interfaces between NiCr and Al_2O_3 particles (Al_2O_3 particle is inside the area) and (b) bonding between Al_2O_3 and NiCr particles. FESEM images

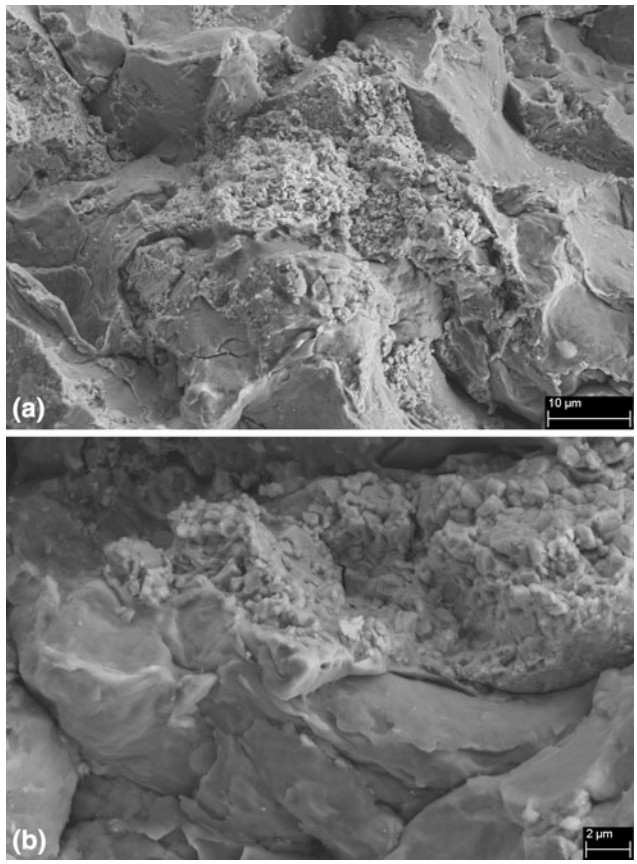

Fig. 12 Fracture surfaces of as-sprayed NiCr + 30WC-Co-Cr-2 coatings (a) general view, (b) bonding between WC-Co-Cr and NiCr particles. FESEM images

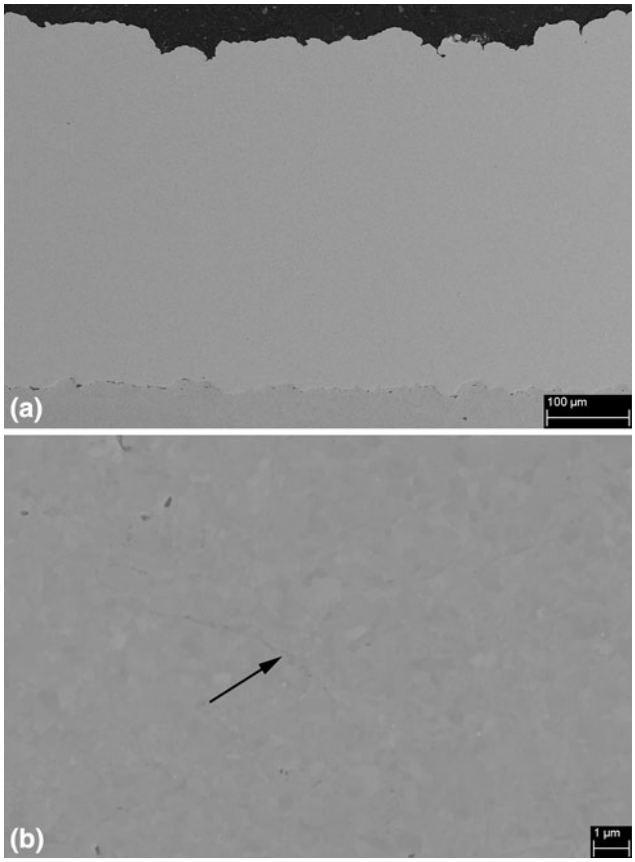

Fig. 13 Cold-sprayed Ni-2 coating in as-sprayed state (a) cross section and (b) microstructure, arrow shows crossing point of three Ni particles. FESEM images

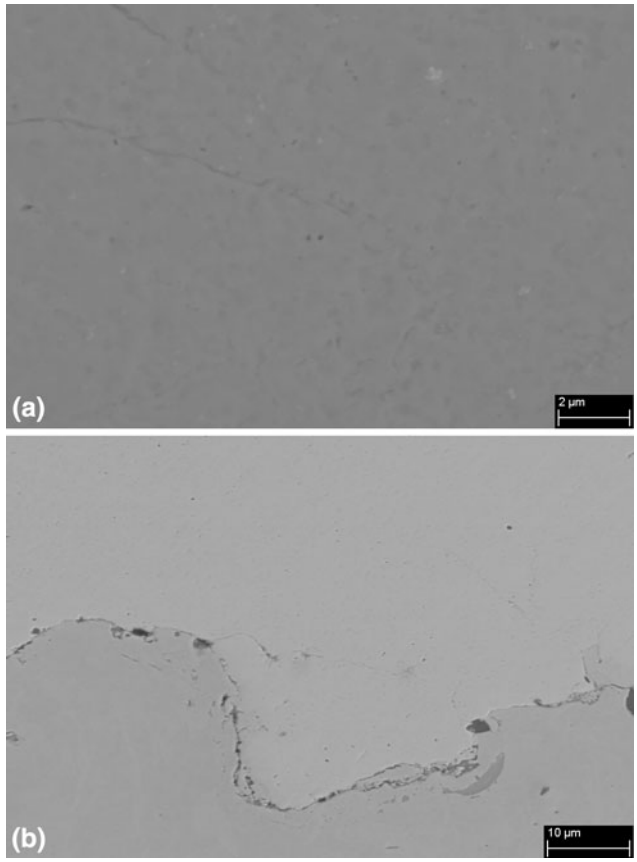

Fig. 14 Cold-sprayed NiCu-2 coating (a) as-sprayed microstructure, oxidized boundaries and (b) heat-treated structure and interface between coating and substrate. FESEM images

coating is presented in Fig. 13. The Ni-2 coating had better structural properties, i.e., denser structure than the Ni-1 coating had. The tight bond between Ni particles in the highly dense coating (Ni-2) is shown by an arrow in Fig. 13(b). The effect of heat treatment was clearly seen in the fracture surfaces, but microstructure did not reveal any more information. The cross section of heat-treated Ni-2 coating was appeared similar with the cross section of as-sprayed coating with very dense structure and without voids or pores.

The cross section of the NiCu-2 coating is presented in Fig. 14. The NiCu-2 coating seemed to be highly dense, defect-free, and faultless. However, slightly oxidized boundaries are still detected in the cross-sectional structures both in the as-sprayed and heat-treated state (Fig. 14a and b, respectively). According to the corrosion tests, NiCu coatings became denser, but still structures contained some weak points which can be explained with these oxidized particle boundaries.

The fracture surfaces of the as-sprayed and heat-treated NiCr-1 coatings already revealed undeformed particles with weak bonding. Additionally, microstructures of these coatings showed that coatings included porosity (Fig. 15a) and open or weak particle boundaries (Fig. 15b) in their structures in the as-sprayed state.

Figure 16 shows microstructure of $NiCr + 50Al_2O_3$-2 coating in the as-sprayed (Fig. 16a and b) and heat-treated state (Fig. 16c). Porosity inside the coating structure was significantly lower in the $NiCr + Al_2O_3$ coatings compared with NiCr coating. The amount of Al_2O_3 particles was 5% according to image analysis (ImageJ). The tight bonding between NiCr and Al_2O_3 particle is perceived in Fig. 16(b). Moreover, some oxidized boundaries are observed in the heat-treated structure (Fig. 16c). However, the amount of oxidized areas was much lower in the metallic-ceramic mixture coating compared with pure metallic coating due to the higher level of plastic deformation occurred on the impacts.

Figure 17 presents the microstructure of NiCr-30WC-Co-Cr-2 coating in the as-sprayed and heat-treated state. The amount of WC-Co-Cr particles was 18% according to image analysis (ImageJ). The structure of NiCr mixture coating included more WC-Co-Cr particles compared with Al_2O_3 particles. Hardmetal particles were not as dense as Al_2O_3 particles in the as-received state, and they deformed and broke down during impacts and thus, more embedded in the metallic structure. The addition of the ceramic particles to the powder-gas flow (Ref 9) or to metallic powder (Ref 14) has reportedly increased the deposition efficiency of the metallic coating due to the

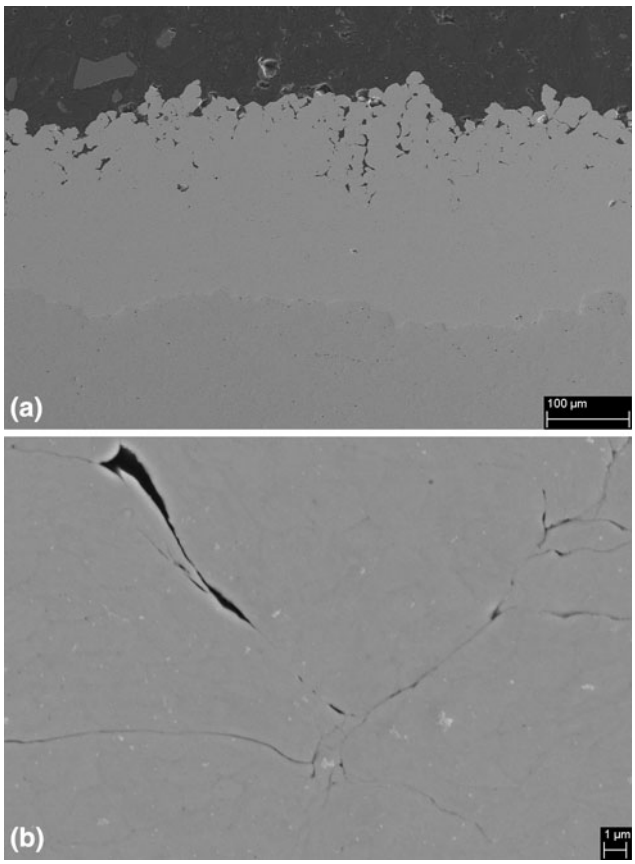

Fig. 15 Cold-sprayed NiCr-1 coating in as-sprayed state (a) cross section and (b) open particle boundaries. FESEM images

activation mechanism of hard particles. The increment of coating thickness compared NiCr coating with NiCr + $50Al_2O_3$ and NiCr + 30WC-Co-Cr coatings were noticeable also in this study, compare coating thicknesses of NiCr (Fig. 15a), NiCr + Al_2O_3 (Fig. 16a), and NiCr + WC-Co-Cr (Fig. 17a) coatings: 250 μm, 331 μm, and 386 μm, respectively.

3.4 Hardness

Vickers hardness was measured in order to characterize the mechanical behavior and hardening of the coatings. In addition, the effect of heat treatments on the properties was performed. Table 4 summarizes the Vickers hardness of the coatings in the as-sprayed and heat-treated state. The hardness measurements of the NiCr + $50Al_2O_3$ and NiCr + 30WC-Co-Cr coatings were done in the metallic areas of the coatings in order to analyze the behavior of metallic particles and hence, the effect of hard particles addition on the metallic area of the coating. Hardness of the Ni and NiCu coatings was significantly decreased after heat treatment due to the fact that coatings were softer state by recovery and recrystallization. However, the hardness of NiCr, NiCr + $50Al_2O_3$, and NiCr + 30WC-Co-Cr coatings were at the same level compared with the

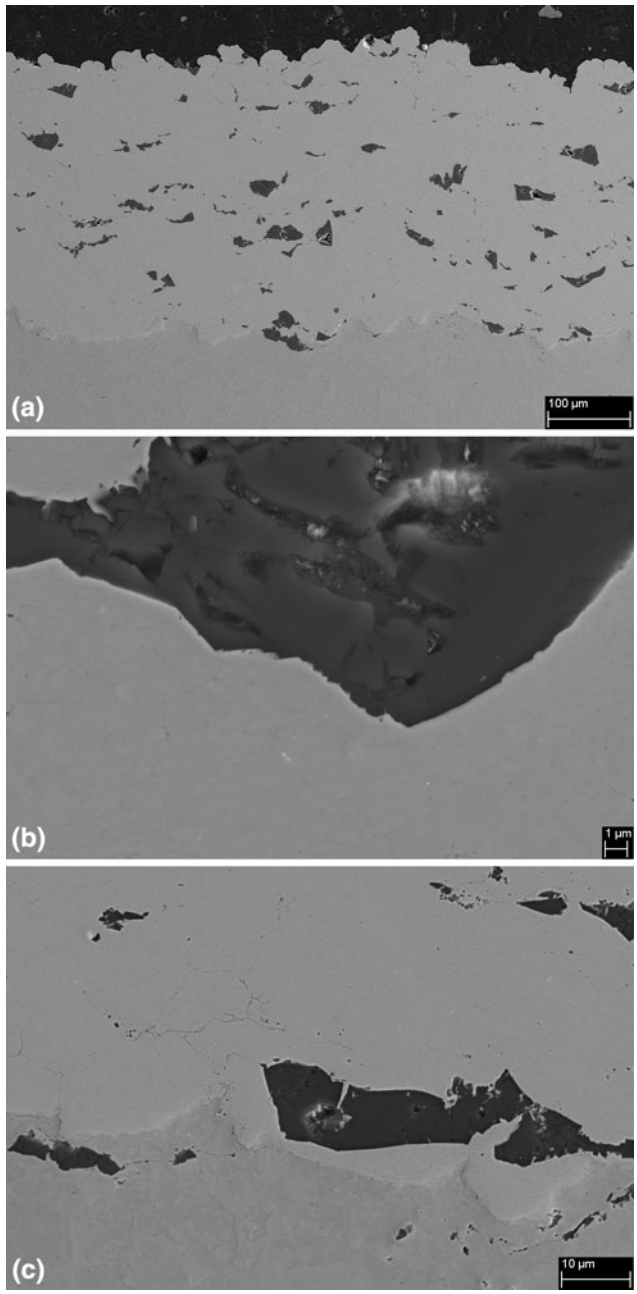

Fig. 16 Cold-sprayed NiCr + $50Al_2O_3$-2 coating (a) as-sprayed cross-sectional structure, (b) bonding between NiCr and Al_2O_3 particles (as-sprayed), and (c) heat-treated structure. FESEM images

as-sprayed and heat-treated each others. This is possibly caused by the oxygen content of the coatings as weak points in the particle boundaries. The effect of oxidized areas was probably higher than recovery and thus, hardness was not decreased after heat treatments. Moreover, the hardness of NiCr with added hard particles was higher than pure NiCr (measurements were done from the metallic part of the coating), reflecting the hardening by hammering effect of hard particles.

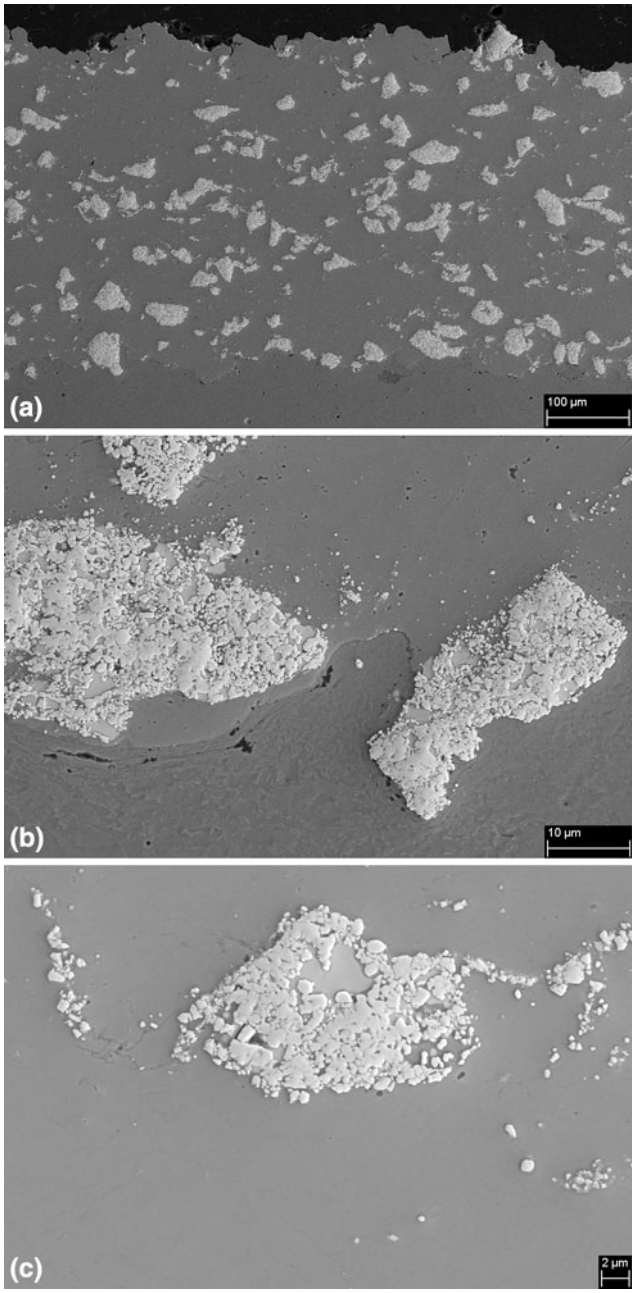

Fig. 17 Cold-sprayed NiCr + 30WC-Cr-Co-2 coating (a) as-sprayed cross-sectional structure, (b) interface between as-sprayed coating and grit-blasted steel substrate, and (c) heat-treated structure. FESEM images

As a summary of the hardness measurements, the hardness of the CS coatings was high due to the work hardening. The hardness was slightly higher in the coatings which were sprayed using lower traverse speed and higher beam distance, indicating high hardening and deformation occurrence. The hard particle addition increased the hardness of the metallic areas of the NiCr + Al_2O_3 and NiCr + WC-Co-Cr coatings. The effect was stronger with Al_2O_3 particles.

Table 4 Vickers hardness ($HV_{0.3}$) of cold-sprayed Ni, NiCu, NiCr, NiCr + 50Al_2O_3, and NiCr + 30WC-Co-Cr coatings in as-sprayed and heat-treated state

	Hardness, $HV_{0.3}$ (SD)	
Coating	As-sprayed	Heat-treated
Ni-1	233 (7.7)	105 (2.8)
Ni-2	238 (5.7)	124 (2.1)
NiCu-1	251 (19.5)	164 (7.5)
NiCu-2	266 (11.3)	185 (14.0)
NiCr-1	247 (31.5)	308 (38.3)
NiCr + 50Al_2O_3-1	375 (42.1)	371 (24.5)
NiCr + 50Al_2O_3-2	398 (46.8)	372 (41.4)
NiCr + 30WC-Co-Cr-1	340 (24.9)	357 (30.6)
NiCr + 30WC-Co-Cr-2	388 (39.7)	387 (40.1)
NiCr + 30WC-Co-Cr-3	337 (29.8)	325 (35.6)
NiCr + 30WC-Co-Cr-4	349 (33.3)	328 (28.9)

4. Discussion

This study shows affecting factors for the denseness of several CS coatings. Coating materials were chosen for their corrosion resistance behavior. Nickel and nickel alloys are known as corrosion resistant materials (Ref 23). However, the corrosion protection of these coatings is based on impermeability and thus, denseness plays very the important role in the corrosion resistance.

4.1 CS Ni Coatings

The denseness of Ni coating was improved significantly due to the optimized powder characteristics together with optimal spraying parameters. Furthermore, the structural details and denseness was affected by heat treatments. Ajdelsztajn et al. (Ref 24) have reported CS nanostructured Ni coating with dense structure according to microscopic analysis. Moreover, in the present study, the highly dense structure of CS Ni coatings was observed with microscopic characterization and in addition, with the corrosion tests. Ni-2 coating had impermeable microstructure without through-porosity in its structure.

The open-cell potential measurements and salt spray tests revealed the impermeability of Ni (Ni-2) coating sprayed with the high-pressure cold spray system. Additionally, the Ni powder was optimized by manufacturer for cold spraying. Furthermore, heat treatments improved the denseness of Ni coatings. The open-cell potential behavior of Ni-2 and HT-Ni-2 coatings was similar with Ni bulk material (Fig. 3), indicating fairly dense coating structure. Moreover, the salt spray test revealed differences in the corrosion behavior of Ni coatings (Table 3). The Ni-2 and HT-Ni-2 coatings contained the rather low amount of corrosion spots on the surface after the salt spray test, 0.8 and 0.1%, respectively. Furthermore, heat treatment decreased the amount of corrosion spots (67.9% Ni-1 and 23.8% HT-Ni-1) in the Ni-1 coatings also, reflecting the densifying effect of heat treatment. The most important affecting factor in the case of CS Ni coatings was optimized spraying parameters. It was observed that the lower

traverse speed of the spraying nozzle together with higher beam distance produced the higher denseness of the coatings. Dense structure requires the high level of plastic deformation and hence, tight bonds between particles. Typically, existing weak points in the CS coatings were concentrated on the weak particle boundaries due to the undeformed particles. In addition, oxide layers were not removed and thus, caused weak bonds between particles.

Particularly, Ni particles were more deformed in the denser coating structure (Fig. 7). The high plastic deformation was observed in the flattened shape of particles. Moreover, tight bonding between three Ni particles (the crossing point of these three particles) was seen in Fig. 7(b) and dense microstructure in Fig. 13(b). The cross section of Ni-2 coating showed defect-free structures and faultless interfaces between coating and substrate. The dense structure of CS coatings depended strongly on the deformation of the particles and hence, the metallic bonds of metallic powder particles (Ref 17, 25). In addition to the spraying parameter optimization, the denseness improvement effect of heat treatments was observed with both Ni coatings (Ni-1 and Ni-2). Heat treatment increased the denseness of Ni-1 coating but did not eliminate all porosity. In addition to the results of corrosion tests and microscopic evaluation, the influence of heat treatment was detected in the hardness measurements. Hardness decreased after heat treatment due to the fact that structure became softer and more ductile (noticed also on the fracture surfaces). Ductile fracturing was dominant in the heat-treated Ni-2 coating (compare Fig. 7 and 8, as-sprayed and heat-treated fracture surfaces). During heat treatment, recrystallization occurred which was seen as decreased hardness values due to the softening.

4.2 CS NiCu Coatings

The denseness improvement was noticeable also in the case of NiCu coatings. Reportedly, particle velocity has strong influence on the coating formation and level of plastic deformation (Ref 4). This was also noticed in this study. Finer particle size ($-30+10$ versus $-38+16$ μm) together with higher process temperature (and advanced spraying system) was found to be better with NiCu powder according to comparison of the results between this present study and our previous study (Ref 22). The highest effect of heat treatment on the denseness improvement was observed with NiCu coatings according to the salt spray test. The amount of corrosion spots was reduced from 54.2% (NiCu-1) to 11.9% (HT-NiCu-1) and 34.7% (NiCu-2) to 11.3% (HT-NiCu-2) after heat treatment. Heat-treated structure was recrystallized and more ductile. The high level of plastic deformation occurred during spraying in the case of NiCu particles. The dense structure formation needs plastic deformation due to the localized shearing (Ref 26). This was seen mostly in NiCu-2 coating (Fig. 9a). Localized shearing is due the hardening by plastic deformation and/or due to the thermal softening caused by heating (Ref 26). However, the structure should be even more ductile in order to be fully dense. For NiCu coating, heat treatment made structure significantly stiffer which was observed on the fracture surfaces (Fig. 9b). In addition, recrystallization was noticed from hardness values by decreased values in comparison with hardness of the as-sprayed and heat-treated coating. This was due to the recrystallization and softening. Additionally, the structures became denser according to the corrosion tests. During recrystallization, the work-hardened structure (with the high amount of dislocations) starts to change positions and new grain structure forms (Ref 26). The same effect as with Ni coatings was observed with these NiCu coatings also.

As well as Ni particles, NiCu particles underwent the high level of deformation due to the thermal softening and adiabatic shear instability (Ref 25). Metal-metal contact under high pressure is the requirement for localized adiabatic shearing and thus, tight bond formation between metallic powder particles (Ref 26). However, in the case of NiCu coating slightly oxidized boundaries were still detected in the cross-sectional structures both in the as-sprayed and heat-treated states. This is due to the fact that oxide layers of powder particles were not totally removed on the particle impacts. According to the corrosion tests, NiCu coatings became denser but still structures contained some weak points which can be explained with these oxidized particle boundaries. As a summary, first, specialized powder characteristics together with optimized spraying parameters led denser coating structure. Second, the densification of NiCu coatings by heat treatment was significant.

4.3 CS NiCr Coatings

It was possible to manufacture NiCr coatings by using cold spraying. However, coatings contained porosity due to the less deformed particles and thus, weak bonds between particles. The highest process temperature (700 °C) was not possible to use due to the fact that NiCr particles clogged the nozzle. For that reason, particles were not underwent as high deformation level as is needed for generating tight bonds between particles and revealing metal-metal bonding between particles. The open particle boundaries together with oxidized boundaries were perceived in the cross sections of NiCr coating as structural defects (Fig. 15). The corrosion tests showed existing through-porosity in the NiCr coating structure (Fig. 5 and Table 3). After the salt spray test, the surface of NiCr coating was strongly corroded with 98.5% amount of corrosion spots. Heat treatment did not have much influence on microstructural details and not improved the denseness of the coating. The NiCr coating contained over-amount defects in its structure and thus, heat treatment was not capable of densify structure enough. However, partly ductile fractures were found in the fracture surface of heat-treated NiCr coating. Weak bonds between particles due to the too low amount of deformation can cause porosity between particle boundaries (Ref 24). In addition to this, the porous layer on the top of the coating is influenced by the fact that the densifying (or tamping) effect of next particles is missing (Ref 20, 24). One solution to densify the CS NiCr coatings is to add

hard particles into the metallic NiCr powder. As it is found out the functions of the hard particles are (1) keep the nozzle clean, (2) activate the sprayed surface, and (3) densify the structure. In this study, we showed the denseness improvement effect of hard, Al_2O_3 and WC-Co-Cr, particles.

4.4 CS NiCr + 50Al_2O_3 Coatings

Typically, a ceramic addition mixed with metallic powder is used in low-pressure cold spraying. Powder mixtures, e.g., Cu + Al_2O_3, Ni + Al_2O_3, Zn + Al_2O_3, and Al + Zn + Al_2O_3 are commercially available (Ref 27). In addition, metal-ceramic composite (e.g., Al-Al_2O_3) coatings have sprayed successfully (Ref 28). Furthermore, we have demonstrated the capability to improve the denseness of high-pressure CS NiCr coating by adding the hard ceramic particles into the metallic NiCr powder. Furthermore, coating thicknesses increased with the hard particle addition, indicating higher deposition efficiency. Powder characteristics are one of the important factors in the cold spraying. Optimal powder properties (e.g., particle size, particle size distribution, and morphology) depend on coating material. According to previous study (Ref 14) added Al_2O_3 particles affected significantly on the microstructural properties of CS NiCr + Al_2O_3 coatings. The best characteristics of Al_2O_3 particles were achieved to be the coarsest particle size (−90 + 45 versus −45 + 22 and −22 + 5 μm) and the highest composition (50 vol.% versus 30 vol.%). Therefore, the particle size of −90 + 45 μm and amount of 50 vol.% were chosen. Moreover, coarser NiCr (−30 + 10 versus −22.5 + 10 μm) particles were used in this study compared with previous study (Ref 14). Moreover, NiCr + Al_2O_3 coatings were heat-treated in order to analyze the effect of annealing.

The corrosion tests demonstrated the densification of NiCr coatings with added Al_2O_3 particles, comparing the results of NiCr and NiCr + Al_2O_3 coatings in both corrosion tests (Fig. 5 and Table 3). The denseness improvement was significant (the amount of corrosion spots on the surfaces of NiCr and NiCr + Al_2O_3 98.5% and 14.1%, respectively). The effect of spraying parameters on the coating formation is material-dependent. In this study, the traverse speed and beam distance combination had the minor effect on the coating formation in the case of NiCr + Al_2O_3 coating. On the other hand, the hard particle addition had the major effect on the coating formation and denseness improvement due to the cleaning, activating, and densifying effects of hard particles. The hammering effect had appeared from the fracture surface (Fig. 11b); indicating the high plastic deformation of NiCr particle due to the localized shear instability and material jets formation. Ceramic particles are more brittle than metallic particles and thus, fracture instead of deform. Fracturing of ceramic particles might be necessary for the coating formation (Ref 10). Fracturing of hard particles was reported (Ref 11). On the other hand, some ceramic particles were embedded in the structure. Furthermore, the oxide layers of metallic particles should also be fractured and removed, revealing metallic surfaces of the particles for metal-metal bonding. Added hard particles help to destroy the oxide layers from metal surfaces by activating, hammering, and tamping the sprayed surfaces. Bonding between metallic and ceramic particles was observed in Fig. 11(b) and 16(b). Sticking between these different material-type particles had occurred by mechanical interlocking due to the embedding of the hard ceramic particles into the softer metallic matrix.

Additionally, heat treatment had influence on the denseness by improving it. Denser coating structures were achieved after heat treatment (see Fig. 5 and Table 3). The amount of corrosion spots was decreased from 14.1% and 12.7% to 7.5% and 8.5% after the salt spray test. However, the effect of heat treatment on microstructure was not significant (Fig. 16) whereas the fracture surface analysis showed slightly more ductile fractures in the heat-treated coating than in the as-sprayed state (Fig. 11a). In addition, the hardness of the metallic part of the coatings were at the same level in both as-sprayed and heat-treated states. With these coatings, recovery occurred during heat treatment which was seen in the slight denseness improvement. However, recrystallization would need higher annealing temperature or longer annealing time. The most important result was denseness improvement of NiCr coating by using hard particles in order to reinforce the structure due to the high level of localized deformation, material jets and adiabatic shear instability.

4.5 CS NiCr + 30WC-Co-Cr Coatings

Hardmetal particles were added into the NiCr powder in order to improve the denseness and corrosion properties compared with the pure NiCr coating. WC-Co-Cr was chosen because of its better corrosion resistance than WC-Co (Ref 29). WC-Co-Cr particles acted like Al_2O_3 particle with three ways: (1) activate the sprayed surface, (2) reinforce the coating structure, and (3) keep the nozzle clean (Ref 14). Coating forms on the solid-state impacts (Ref 2) and no melting of WC-Co particles during impacts were observed (Ref 12). Hard particle addition makes possible to use higher gas temperature, which affects particle velocity by increasing it (Ref 10). On the other hand, higher particle velocity leads stronger deformation and thus, denser coating structure. The effect of preheating temperature of gas on the denseness of NiCr + WC-Co-Cr coatings was significant according to the corrosion tests (Fig. 6 and Table 3). The highest temperature (700 °C) led the lowest porosity into the coatings. The reason for that was the higher velocity causes higher deformation and thus, denser structure. In addition, void reduction occurs with high deformation (Ref 10). In addition to the process temperature, open-cell potential measurements showed that lower traverse speed together with higher beam distance had remarkable effect on the denseness of the coating.

The fracture surface analysis revealed the high level of deformation of NiCr particles whereas hardmetal particles were broken down and fragmented. Therefore, hardmetal particles were placed all over the coating structure (Fig. 12). Lee et al. (Ref 28) were found out the same kind

of occurrence were hard particles fragmented during impact. They have used agglomerated Al_2O_3 whereas we used sintered and crushed WC-Co-Cr particles. Heat treatment had only minor effect in the case of NiCr + WC-Co-Cr coating. After heat treatment, the fracture surface of the coating was slightly more ductile. In addition, the hardness of the as-sprayed and heat-treated NiCr + WC-Co-Cr coatings were similar, reflecting only the minor effect of heat treatment. Only the lower traverse speed and higher beam distance combination caused higher hardness, indicating the higher level of work hardening and plastic deformation.

Microstructures of NiCr + 30WC-Co-Cr coatings were dense without noticeable pores or other defects (Fig. 17). Moreover, the structure of NiCr + 30WC-Co-Cr coating contained more added hard particles than NiCr + Al_2O_3 coating in proportion to initial powder compositions. WC-Co-Cr particles were more deformed, fell to parts, and stuck to the previous particles and thus, more entered into the structure. Summing up, the metallic structure of NiCr coating can be densified with hardmetal particles. However, spraying parameters had strong influence on the coating formation. High process temperature with lower traverse speed together with higher beam distance was needed in order to produce highly dense coating structure.

5. Conclusions

Cold spraying is proven to be an optimal thermal spray method in order to prepare fully dense or low-porosity coatings from metallic or metallic-ceramic composite mixture powder feedstock. This study showed that structural details, i.e., microstructure, fracture behavior, and denseness, and hardness depend strongly on powder characteristics, spraying parameters, and post-treatments. In optimal situation, fully dense coating structures are able to manufacture with the optimal combination of powder and spraying parameters. In this study, the Ni (Ni-2) coating had overall dense structure. In the contrast to this, sometimes when the optimal combination was not achieved, then structural details can be improved with post-treatments. In this study, the denseness improvement of NiCu coatings was done with heat treatments. Heat-treated NiCu coatings were the softer state due to the recrystallization and structures became denser according to the corrosion tests. In addition to these, one solution to decrease through-porosity is powder mixing. Hard particle addition into the metallic powder has shown significant denseness improvement. This was clarified with NiCr coatings added hard particles (NiCr + 50Al_2O_3 and NiCr + 30WC-Co-Cr). Al_2O_3 particles embedded in the structure of NiCr coatings whereas WC-Co-Cr particles broke down and stuck into the structure. Both particle additions made the structure of NiCr coating denser due to the fact that higher gas temperature was able to use and due to the hammering and tamping of the coating structure.

Acknowledgments

The authors thank Mr. Werner Krömmer of Linde AG Gas for spraying the coatings and for his valuable advice. They also thank Mr. Jonne Näkki of KETEK for the salt spray tests. The project was funded by Academy of Finland and Finnish Graduated School of New Materials and Processes.

References

1. T. Schmidt, F. Gärtner, H. Assadi, and H. Kreye, Development of a Generalized Parameter Window for Cold Spray Deposition, *Acta Mater.*, 2006, **54**, p 729-742
2. H. Assadi, F. Gärtner, T. Stoltenhoff, and H. Kreye, Bonding Mechanism in Cold Gas Spraying, *Acta Mater.*, 2003, **51**, p 4379-4394
3. M. Grujicic, C.L. Zhao, W.S. DeRosset, and D. Helfritch, Adiabatic Shear Instability Based Mechanism for Particles/Substrate Bonding in the Cold-Gas Dynamic-Spray Process, *Mater. Des.*, 2004, **25**, p 681-688
4. A. Papyrin, V. Kosarev, S. Klinkov, A. Alkimov, and V. Fomin, *Cold Spray Technology*, 1st ed., Elsevier, the Netherlands, 2007, p 328
5. R. Maev and V. Leshchynsky, Air Gas Dynamic Spraying of Powder Mixtures: Theory and Application, *J. Therm. Spray Tech.*, 2006, **15**(2), p 198-205
6. H. Koivuluoto, J. Näkki, and P. Vuoristo, Corrosion Properties of Cold-Sprayed Tantalum Coatings, *J. Therm. Spray Tech.*, 2009, **18**(1), p 75-82
7. T. Van Steenkiste and D.W. Gorkiewicz, Analysis of Tantalum Coatings Produced by the Kinetic Spray Process, *J. Therm. Spray Tech.*, 2004, **13**(2), p 265-273
8. T.S. Price, P.H. Shipway, D.G. McCartney, E. Calla, and D. Zhang, A Method for Characterizing the Degree of Inter-particle Bond Formation in Cold Sprayed Coatings, *J. Therm. Spray Tech.*, 2007, **16**(4), p 566-570
9. S.V. Klinkov, V.F. Kosarev, A.A. Sova, and I. Smurov, Calculation of Particle Parameters for Cold Spraying of Metal-Ceramic Mixtures, *J. Therm. Spray Tech.*, 2009, **18**(5-6), p 944-956
10. T.H. Van Steenkiste, J.R. Smith, and R.E. Teets, Aluminum Coatings Via Kinetic Spray with Relatively Large Powder Particles, *Surf. Coat. Technol.*, 2002, **154**, p 237-252
11. H.Y. Lee, Y.H. Yu, Y.C. Lee, Y.P. Hong, and K.H. Ko, Cold Spray of SiC and Al_2O_3 with Soft Metal Incorporation: A Technical Contribution, *J. Therm. Spray Tech.*, 2004, **13**(2), p 184-189
12. R.S. Lima, J. Karthikeyan, C.M. Kay, J. Lindemann, and C.C. Berndt, Microstructural Characteristics of Cold-Sprayed Nanostructured WC-Co Coatings, *Thin Solid Films*, 2002, **416**, p 129-135
13. H.-J. Kim, C.-H. Lee, and S.-Y. Hwang, Fabrication of WC-Co Coatings by Cold Spray Deposition, *Surf. Coat. Technol.*, 2005, **191**, p 335-340
14. H. Koivuluoto and P. Vuoristo, Effect of Ceramic Particles on Properties of Cold-Sprayed Ni-20Cr + Al_2O_3 Coatings, *J. Therm. Spray Tech.*, 2009, **18**(4), p 555-562
15. A. Shkodkin, A. Kashirin, O. Klyuev, and T. Buzdygar, The Basic Principles of DYMET Technology, *Thermal Spray 2006: Pushing the Envelope of Materials Performance*, B.R. Marple, M.M. Hyland, Y.C. Lau, R.S. Lima, and J. Voyer, Ed., May 15-18, 2006 (Seattle, Washington, USA), ASM International
16. R. Maev and V. Leshchynsky, *Introduction to Low Pressure Gas Dynamic Spray, Physics & Technology*, Wiley-VCH Verlag GmbH & Co, KGaA, Weinheim, Germany, 2008, p 328
17. M. Grujicic, J.R. Saylor, D.E. Beasley, W.S. DeRosset, and D. Helfritch, Computational Analysis of the Interfacial Bonding Between Feed-Powder Particles and the Substrate in the

Cold-Gas Dynamic-Spray Process, *Appl. Surf. Sci.*, 2003, **219**, p 211-227
18. V.K. Champagne, Ed., *The Cold Spray Materials Deposition Process, Fundamentals and Applications*, Woodhead publishing Limited, Cambridge, England, 2007, p 362
19. T.H. Courtney, *Mechanical Behavior of Materials*, McGrae-Hill Publishing Company, Singapore, 1990, p 710
20. H. Mäkinen (Koivuluoto), J. Lagerbom, and P. Vuoristo, Mechanical Properties and Corrosion Resistance of Cold Sprayed Coatings, *Thermal Spray 2006: Pushing the Envelope of Materials Performance*, B.R. Marple, M.M. Hyland, Y.C. Lau, R.S. Lima, and J. Voyer, Ed., May 15-18, 2006 (Seattle, Washington, USA), ASM International, 6 p
21. H. Mäkinen (Koivuluoto), J. Lagerbom, P. Vuoristo, Adhesion of Cold Sprayed Coatings: Effect of Powder, Substrate, and Heat Treatment, *Thermal Spray 2007: Global Coating Solutions*, B. Marple, M. Hyland, Y.-C. Lau, C.-J. Li, R. Lima, and G. Montavon, Ed., ASM International, May 14-16, 2007 (Beijing, China), p 31-36
22. H. Koivuluoto, J. Lagerbom, and P. Vuoristo, Microstructural Studies of Cold Sprayed Copper, Nickel, and Nickel-30%Copper Coatings, *J. Therm. Spray Tech.*, 2007, **16**(4), p 488-497
23. P. Crook, Corrosion of Nickel and Nickel-Base Alloys, *Corrosion: Materials*, Vol. 13B, *ASM Handbook*, ASM International, 2005, p 228-251
24. L. Ajdelsztajn, B. Jodoin, and J.M. Schoenung, Synthesis and Mechanical Properties of Nanocrystalline Ni Coatings Produced by Cold Gas Dynamic Spraying, *Surf. Coat. Technol.*, 2006, **201**, p 1166-1172
25. T. Stoltenhoff, C. Borchers, F. Gärtner, and H. Kreye, Microstructures and Key Properties of Cold-Sprayed and Thermally Sprayed Copper Coatings, *Surf. Coat. Technol.*, 2006, **200**, p 4947-4960
26. M. Meyers, Plasticity: Adiabatic Shear Localization, *Encyclopedia of Materials: Science and Technology*, p 7093-7103
27. Obninsk Center for Powder Spraying, Website: http://www.amazonit.ru/ocpn/eindex.html
28. H.Y. Lee, S.H. Jung, S.Y. Lee, Y.H. You, and K.H. Ko, Correlation Between Al_2O_3 Particles and Interface of Al-Al_2O_3 Coatings by Cold Spray, *Appl. Surf. Sci.*, 2005, **252**, p 1891-1898
29. L.-M. Berger, P. Ettmayer, P. Vuoristo, T. Mäntylä, and W. Kunert, Microstructure and Properties of WC-10%Co-4%Cr Spray Powders and Coatings: Part 1. Powder Characterization, *J. Therm. Spray Tech.*, 2001, **10**(2), p 311-325